Flame-Retardant Polypropylene/Multiwall Carbon Nanotube Nanocomposites: Effects of Surface Functionalization and Surfactant Molecular Weight

Qingliang He, Tingting Yuan, Xingru Yan, Daowei Ding, Qiang Wang, Zhiping Luo, Tom D. Shen, Suying Wei,* Dapeng Cao,* Zhanhu Guo*

Flame-retardant polypropylene (PP)/carbon nanotubes (CNTs) nanocomposites influenced by surface functionalization and surfactant molecular weights are studied. 3-Aminopropyl-triethoxysilane (APTES) is utilized to modify the CNTs (f-CNTs), and maleic-anhydride-grafted PP (MAPP) with two molecular weights ($\bar{M}_n$ of 800 and 8000 g mol^{-1}) is used to further improve the dispersion of f-CNTs in the PP matrix. Thermal gravimetric analysis (TGA) and microscale combustion calorimetry (MCC) reveal that the molecular weight of MAPP directly affects the thermal stability and flammability of PP/f-CNTs PNCs: both MAPP polymers ($\bar{M}_n$ of 800 and 8000 g mol^{-1}) increase the thermal stability of PP; however, the heat release rate of PP/f-CNTs is reduced in the presence of MAPP ($\bar{M}_n$ of 800 g mol^{-1}) and increased in the presence of MAPP ($\bar{M}_n$ of 8000 g mol^{-1}). MAPP ($\bar{M}_n$ of 800 g mol^{-1}) also results in a lower viscosity of the PP/f-CNTs PNCs compared with pure PP.

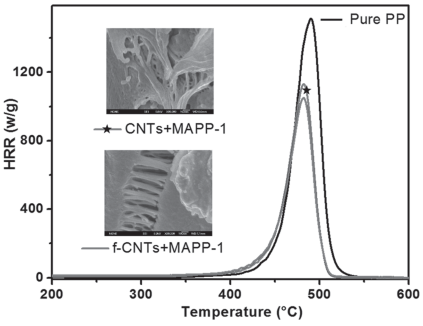

1. Introduction

Carbon nanotubes (CNTs) were considered as one of the most promising nanomaterials and have been extensively investigated due to their unique mechanical,[1–4] electrical,[5] and optical[6,7] properties, and their superior energy storage,[8–10] thermal stability, and flame-retardancy behaviors.[11–15] Therefore, the multifunctional polymer nanocomposites (PNCs) reinforced with CNTs have been prepared due to the aforementioned merits.[16–23] However, owing to the inert surface and large specific surface area of CNTs, agglomeration and limited compatibility of CNTs with polymer matrices are two major challenges to impede obtaining well-dispersed CNTs

Q. He, Dr. T. Yuan, X. Yan, D. Ding, Prof. S. Wei, Prof. Z. Guo, Integrated Composites Laboratory (ICL), Dan F. Smith Department of Chemical Engineering, Lamar University, Beaumont, TX 77710, USA
E-mail: suying.wei@lamar.edu; zhanhu.guo@lamar.edu
Q. He, Prof. S. Wei
Department of Chemistry and Biochemistry, Lamar University, Beaumont, TX 77710, USA
Prof. Q. Wang
College of Environmental Science and Engineering, Beijing Forestry University, Beijing 100083, China
Prof. Z. Luo
Department of Chemistry and Physics and Southeastern North Carolina Regional Microanalytical and Imaging Consortium, Fayetteville State University, Fayetteville, NC 28301, USA
Prof. T. D. Shen
Nanostructured & Amorphous Materials, Inc., Houston, TX 77084, USA
Prof. D. Cao
State Key Laboratory of Organic–Inorganic Composites, Beijing University of Chemical Technology, Beijing 100029, China
E-mail: caodp@mail.buct.edu.cn

© 2014 WILEY-VCH Verlag GmbH & Co. KGaA, Weinheim

DOI: 10.1002/macp.201300608

reinforced PNCs.[17] To achieve uniform dispersion in the hosting polymer matrix, extensive researches have been carried out to functionalize CNTs aiming to form strong chemical bonding with the polymer.[24–29] It has been reported that the electrical,[30,31] mechanical,[24,32] rheological,[33] and thermal properties[34–37] can be improved considerably when functionalized CNTs are finely dispersed in the polymer matrix.

Among all types of thermoplastics, polyolefin-based PNCs containing CNTs usually encounter severe dispersion quality issue due to: weak interfacial adhesion between the inert nonpolar hydrocarbon backbones and the inert CNT surfaces; and high surface energy and strong intermolecular interactions among the nanosized CNTs.[25,28] Two approaches are normally used to improve the dispersion quality in polyolefin matrix. The first is to generate functional groups on the surface of CNTs through using end-group functionalization,[38–40] ionic surfactants,[41] or plasma coating,[26,42] which enhance the affinity of CNTs to polymer backbones;[43] and the second is to introduce reactive sites on the polymer matrix (such as grafting maleic anhydride through Alder ENE reaction)[44] in order to improve the compatibility with CNTs.

As an alternative to grafting functional groups on the macromolecular polyolefins directly, low-molecular-weight polyolefin-based compatibilizer/coupling agents have been widely used to improve the polymer-filler compatibility.[45–49] Maleic-anhydride-grafted polypropylene (MAPP) is commonly used as a coupling agent between the polymer matrix and the nanofillers including organoclay,[50] double-layered hydroxides,[51] and CNTs.[52] Due to the similarity in backbone structure as polyolefin, MAPP is highly miscible to polyolefin-based matrix. In addition, its MA functional groups, capable of bonding many kinds of nanofillers to significantly decrease the surface tension at the polymer–filler interface, can thus effectively prevent the agglomeration of nanofillers. The concentration effect of MAPP on improving the dispersion quality of different nanofillers in polymer matrix and thus increasing their compatibility have been well studied.[53] However, how the surfactant (i.e., MAPP) molecular weight affects the structure and property of the PNCs filled with CNTs is still not clear and have been rarely reported yet.

In this work, a facile ex situ solution-based mixing method was employed to prepare the PP/CNTs PNCs. The surface of hydroxyl (OH) CNTs was modified with silane coupling agent-3-aminopropyltriethoxysilane (APTES) in order to introduce functional groups and two different MAPP ($\bar{M}_n$ of ca. 800 and 8000 g mol^{-1}) were used as surfactant to further aid the dispersion of the functionalized CNTs in PP matrix. The functionalization of CNTs was characterized by transmission electron microspectroscopy (TEM) and Fourier transform infrared (FTIR) spectroscopy; meanwhile, the dispersion quality of the CNTs in the PP matrix was evaluated by scanning electron microscopy (SEM). The physical properties of the PP/CNTs affected by the surface functionalization of CNTs and the aids of surfactant MAPP with different molecular weights were demonstrated through investigating the thermal properties (thermogravimetric analysis, differential scanning calorimetry), flame-retardant performance (microscale combustion calorimetry), and melting rheological behaviors.

2. Experimental Section

2.1. Materials

Isotactic PP (ρ = 0.9 g cm^{-3}, $\bar{M}_n \approx$ 40 500 g mol^{-1}, $\bar{M}_w \approx$ 155 000 g mol^{-1}) was supplied by Total Petrochemicals USA, Inc. The OH-functionalized multiwall carbon nanotubes (CNTs) (–OH content: 0.67–0.75 wt%, purity: >95%, specific surface area: 60–80 m^2 g^{-1}, average outer diameter of 50–80 nm, inside diameter of 5–15 nm, and length of 10–20 μm) were supplied by Nano-structured and Amorphous Materials, Inc, Houston, Texas.

Two MAPPs (provided by Baker Hughes Inc) were utilized: 1) MAPP-1 ($\bar{M}_n \approx$ 800 g mol^{-1}) was a gel-like propylene-hexene copolymer with one maleic anhydride (MA) group at one terminal through Alder–ENE reaction,[44] and the other MA group grafted on the main chain; and 2). MAPP-2 ($\bar{M}_n \approx$ 8000 g mol^{-1}) was also a solid homo-polypropylene with one terminal MA group and the other MA group grafting on the main chain (structures shown in Scheme 1). 3-Aminopropyl-triethoxysilane (APTES) (chemical structure shown in Scheme 1) was purchased from Sigma–Aldrich (purity of 99%). Solvent xylene (laboratory grade, boiling point: ≈140 °C, ρ = 0.87 g cm^{-3}) and concentrated nitric acid (HNO_3) were purchased from Fisher Scientific. All of the chemicals were used as-received without any further treatment.

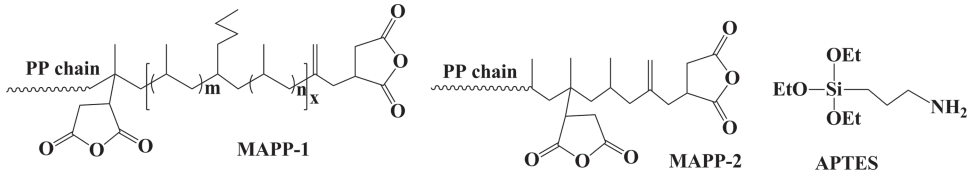

Scheme 1. Chemical structures of MAPP-1 ($\bar{M}_n$ = 800 g mol^{-1}), MAPP-2 ($\bar{M}_n$ = 8000 g mol^{-1}) and APTES.

© 2014 WILEY-VCH Verlag GmbH & Co. KGaA, Weinheim

2.2. Modification of CNTs and Synthesis of Polymer Nanocomposites

The surface of the CNTs was modified by APTES. Briefly, CNTs (1.0 g) were dispersed in 100 mL xylene in a 250 mL three-neck round-bottom flask under ultrasonication for 2 h. The flask was then transferred to a heating mantle to heat the mixture to reflux (≈140 °C). APTES (10.0 wt% of CNTs) was then added in the solution dropwisely and the mixture was refluxed for an additional 8 h in order to finish the silanization reaction. After that, the solution was suction-filtered and the obtained residue was washed several times with DI water, ethanol, and acetone in sequence for three times. The functionalized CNTs (denoted as f-CNTs) were finally obtained after the residue was dried in a vacuum oven at 80 °C overnight.

The PP PNCs filled with 1.0 wt% CNTs (or f-CNTs) in the presence/absence of MAPP was prepared from an ex situ solution blending method. Briefly, 9.9 g PP pellets (or a mixture of 9.8 g PP pellets and 0.1 g MAPP) was dissolved in 100 mL xylene in a 500 mL three-neck round-bottom flask by refluxing xylene at ≈140 °C. At the same time, 0.1 g CNTs or f-CNTs (or a mixture of 0.1 g CNTs/f-CNTs and 0.1 g MAPP) was dispersed in 30 mL xylene under 2 h ultrasonication to form a colloidal solution. The colloidal solution was then transferred to the flask, and the final mixture was mechanically stirred (300 rpm) for additional 2 h to ensure the dispersion quality at 140 °C. Finally, the solid samples were extracted by pouring hot colloidal solution (containing PP and CNTs/f-CNTs in the presence/absence of MAPP) to ice water for phase separation, and dried overnight at room temperature in the fume hood to form black powders. The final composite powders were obtained from drying the black powders in a vacuum oven at room temperature overnight.

The testing samples were prepared from reshaping the composite powders using hot press molding machine (Model: Carver 3853–0, USA). The brief procedures were as follows. The composite powders were added in a cylinder-shaped mold, which was then placed between two panels in the molding machine. The mold was then heated to 180 °C at a heating rate of 20 °C min^{-1} under the pressure of 10 MPa and maintained at 180 °C for 5–10 min. Finally, the plate-shape sample was cooled down naturally to room temperature in the mold.

2.3. Characterization

Fourier transform infrared spectroscopy (Bruker Alpha spectrometer) with a Hyperion 1000 attenuated total reflection (ATR) microscopy accessory was used to characterize the PP matrix and its PNCs over the wavenumber range from 4000 to 500 cm^{-1} at a resolution of 4 cm^{-1}.

Transmission electron microscope (TEM) was used to determine the dispersion of CNTs in the as-prepared PP PNCs in an FEI TECNAI G2 F20 microscope at a working voltage of 200 kV. The samples were prepared from the hot solution of the PP PNCs at the end of the synthesis process. One droplet of the diluted hot solution containing the MWNTs was dropped on a 400-mesh carbon-coated copper grid (Electron Microscopy Sciences).

The chemical environment of the untreated CNTs and f-CNTs was further studied by X-ray photoelectron spectroscopy (XPS) on a Kratos AXIS 165 system. The scan of each sample was carried out with a monochromatic Al X-ray source at the anode of 10 kV and beams current of 15 mA.

For the microstructural examination in the scanning electron microscopy (SEM), the samples were mounted on an aluminum stub by using carbon tape and then sputtered in a Hummer 6.2 system (15 mA AC for 30 s), creating approximately a one-nanometer film of Au. The scanning electron microscope used was a JEOL JSM 6700R in high-vacuum mode. The images were taken at 5 kV at different magnifications.

Differential scanning calorimetry (DSC) was carried out on a TA Instruments Q2000 calorimeter. Approximately 5 mg sample was encapsulated in an aluminum pan and heated from 30 to 200 °C at a heating rate of 10 °C min^{-1} under a nitrogen flow rate of approximately 50 mL min^{-1}, then cooled down to room temperature after stayed at 200 °C for 1 min to remove the heat history. After that, the samples were reheated again from 30 to 200 °C. The data enclosed here were collected from the first cooling and the second heating cycles.

The thermal stability of pure PP and its PNCs was measured using thermogravimetric analysis (TGA) (TA Instruments Q-500). The samples were heated from room temperature to 700 °C at a constant heating rate of 20 °C min^{-1} under air and nitrogen gas atmosphere, respectively. The flow rate is 60 mL min^{-1} under both two atmospheres.

Microscale combustion calorimetry (MCC) was utilized to determine/assess the flammability/fire hazards by measuring the heat-release-related parameters. To be specific, the heat release capacity (HRC), rate of heat release (HRR) at different temperatures, peak rate of heat release (PHRR), and temperature at PHRR (T_{PHRR}) will be obtained from MCC. Meanwhile, full width half height (FWHH) will be calculated. Here, the data were recorded according to a standard method ASTM D7309-2007 (Method A) using a "MCC-2" calorimeter produced by Govmark Inc. In a typical measurement, about 5 mg sample was heated from 80 to 650 °C using a heating rate of 1 °C s^{-1} in a continuous stream of nitrogen flowing at 80 mL min^{-1}. The thermal decomposition products (also named as "fuel gases") were mixed with a 20 mL min^{-1} stream of oxygen before entering a 900 °C combustion furnace to complete the non-flaming combustion.

Melt rheological behaviors of the PP matrix and its PNCs were studied using TA Instruments Rheometer (model AR 2000ex). Environmental test chamber (ETC) steel parallel-plate geometry (25 mm in diameter) was used to perform the measurement. A dynamic strain sweep at 1 rad s^{-1} was performed in order to find out the limit of linear viscoelasticity. Then, the dynamic oscillation frequency was swept from 100 to 0.1 Hz in the linear viscoelastic range with a strain of 1% at 200 °C under N_2 atmosphere. The samples used are 25 mm in diameter with around 2 mm thickness prepared from hot press mold.

3. Results and Discussion

3.1. Structural and Morphological Characterization

The surface modification by APTES is to introduce amino groups (–NH_2) on the surface of CNTs and thus the functionalized CNTs (f-CNTs) can react with the MA functional

© 2014 WILEY-VCH Verlag GmbH & Co. KGaA, Weinheim

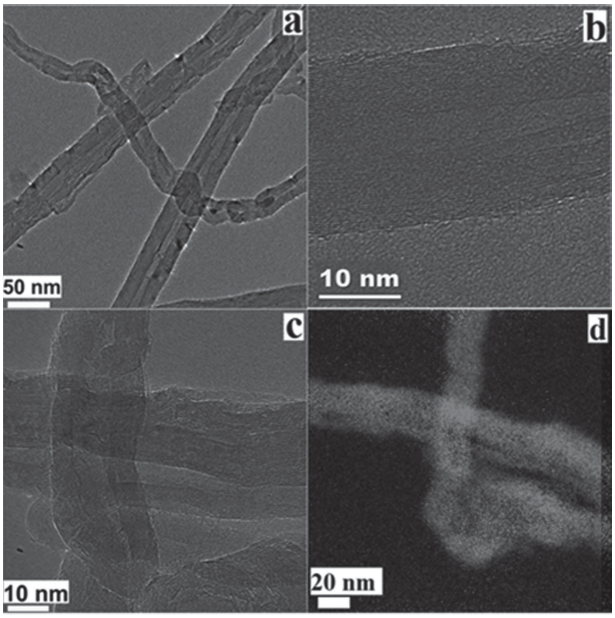

Figure 1. TEM images of: a,b) as-received CNTs. c) f-CNTs, and d) elemental mapping of f-CNTs (carbon: grey, oxygen: outer surface of grey tube structure, silicon: interface between the grey and black colors).

groups in MAPP, which further result in the enhanced interfacial compatibility between CNTs and PP matrix, and the improvement in dispersion quality of f-CNTs in the PP matrix. Figure 1 depicts the TEM microstructures of the as-received CNTs and the f-CNTs.

As shown in Figure 1a,b, the as-received CNTs demonstrated a slightly rough surface, which is attributed to the pre-treatment in introducing the hydroxyl groups on the surface of CNTs. A thin layer covered on the surface of CNTs was observed in the f-CNTs (Figure 1c). A closer observation from the elemental mapping result (Figure 1d) clearly demonstrated a silicon-layer (at the interface between the grey and black colors in the figure) coated on the surface of f-CNTs. This indicated that the outer surface of f-CNTs has been successfully coated with APTES. The oxygen element can also be observed only on the near surface of f-CNTs.

X-ray photoelectron spectroscopy (XPS) was further utilized to study the chemical environment of untreated CNTs and f-CNTs (APTES-treated CNTs). Upon the deconvolution of the C1s peak of the as-received CNTs (Figure 2a), a main peak at 284.7 eV was observed, which is apparently attributed to the graphitic carbon in the tube structure.[54] In addition, other two peaks were attributed to the defects on carbon atoms attached to different oxygen-containing moieties, i.e., a strong C–O peak at ≈286.3 eV and a weak O–C=O peak at ≈289.0 eV.[54] This indicates that the pre-treatment of the as-received CNTs has introduced both hydroxyl and carboxyl groups on the tube surface. After

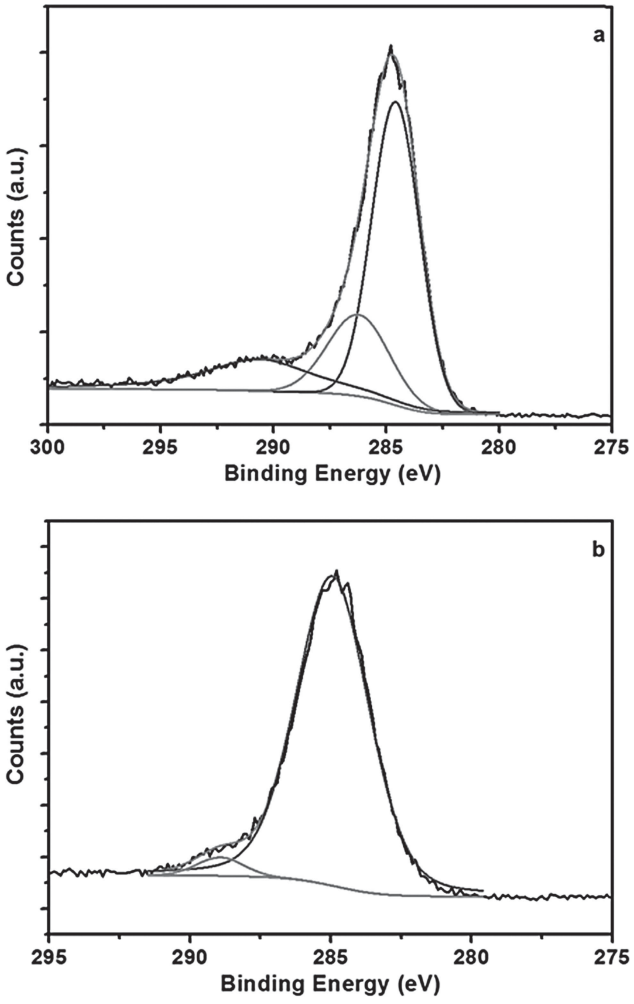

Figure 2. XPS C1s spectra of: a) as-received CNTs, and b) APTES-treated CNTs.

reacting with APTES, the hydroxyl groups were depleted as evidenced by the absence of C–O peak from XPS C1s spectrum (Figure 2b). It can thus be concluded that the APTES was chemically bound onto the f-CNTs.

After adding 1.0 wt% CNTs in the PP matrix, no obvious change was observed (Figure 3a), indicating the weak interaction between the as-received CNTs and the PP molecular chains. When PP was filled with a combination of 1.0 wt% CNTs and 1.0 wt% MAPP (Type 1 or 2), a thicker outer layer on the surface of CNTs was observed (Figure 3b,c). When treated with APTES, the hydroxyl groups on the surface of CNTs will react with the ethoxy-groups of APTES to form covalent bonding (CNTs–O–Si).[55] Upon adding the f-CNTs in the MAPP-xylene solution, amide bond (O=C–N–H) can be formed through the NH_2-groups on the surface of f-CNTs reacting with maleic anhydride on the main chain of MAPP.[56] Therefore, it can be concluded that the f-CNTs can be bound with MAPP (Type 1 or 2), and the compatibility between the f-CNTs

© 2014 WILEY-VCH Verlag GmbH & Co. KGaA, Weinheim

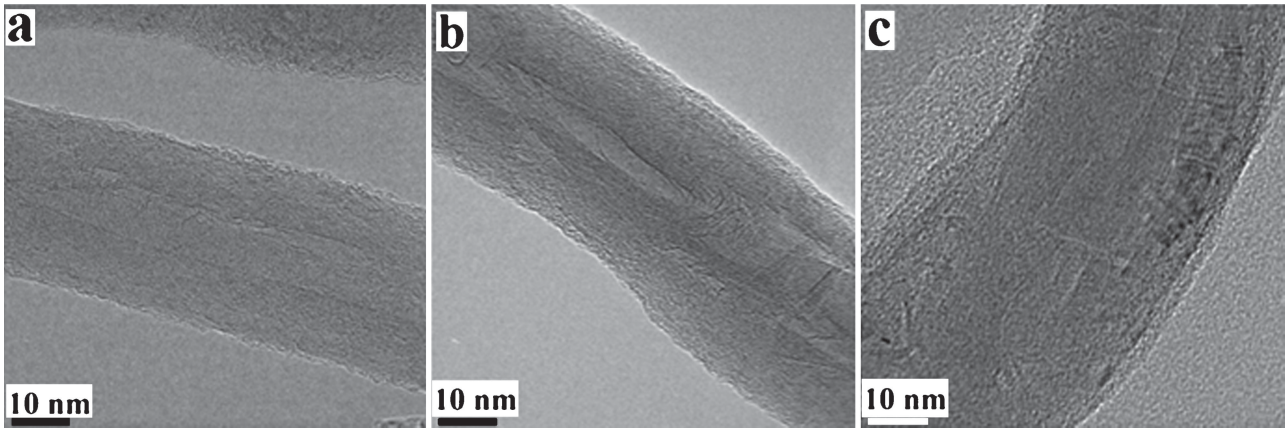

Figure 3. TEM microstructures of: a) PP/1.0% CNTs. b) PP/1.0% CNTs/1.0% MAPP-1, and b) PP/1.0% CNTs/1.0% MAPP-2.

and the hosting inert PP matrix can be enhanced through the bridging effect of MAPP. The reactions are illustrated in Scheme 2.

A thin layer on the surface of f-CNTs was observed when 1.0% f-CNTs was distributed in the PP matrix (Figure 4a,b). Meanwhile, when adding a combination of 1.0% MAPP-1 with 1% f-CNTs in the PP matrix, a thicker coating on the surface of the f-CNTs can be observed (Figure 4c,d). In addition to a thin silicon-coating (shown as light grey on the tube surface from the elemental mapping, insert of Figure 4d), bulk oxygen mapping distribution (black) on the outer surface of the silicon-coating indicates that the oxygen-containing polymers were coated on the silicon layer. This suggests that the MAPP has tightly "wrapped" on the f-CNTs. Meanwhile, when combining the 1.0% f-CNTs with 1.0% MAPP-2 in the PP matrix, a similar layer was observed (Figure 4e,f).

Figure 5 shows the FTIR spectra of pure PP and its PNCs. The peaks at 1450 and 1368 cm^{-1} are attributed to the C–H bending vibration absorption of PP backbone, while the multi peaks around 3000 cm^{-1} are indexed to the absorption of C-H stretching vibration.[57] All these characteristic peaks are well maintained in the PP/1.0 wt% f-CNTs PNCs in the presence of MAPP (Type 1 or 2), indicating that no visible change of PP matrix can be found through adding MAPP and f-CNTs in the PP matrix. It must be noted that a small new peak at around 1000–1100 cm^{-1} (shown in the dashed rectangular area and the enlarged in the insert area) is observed for the PP/1% f-CNTs PNCs and is obviously due to the Si-O bond stretch mode from the successfully bonded APTES on the surface of f-CNTs.[58]

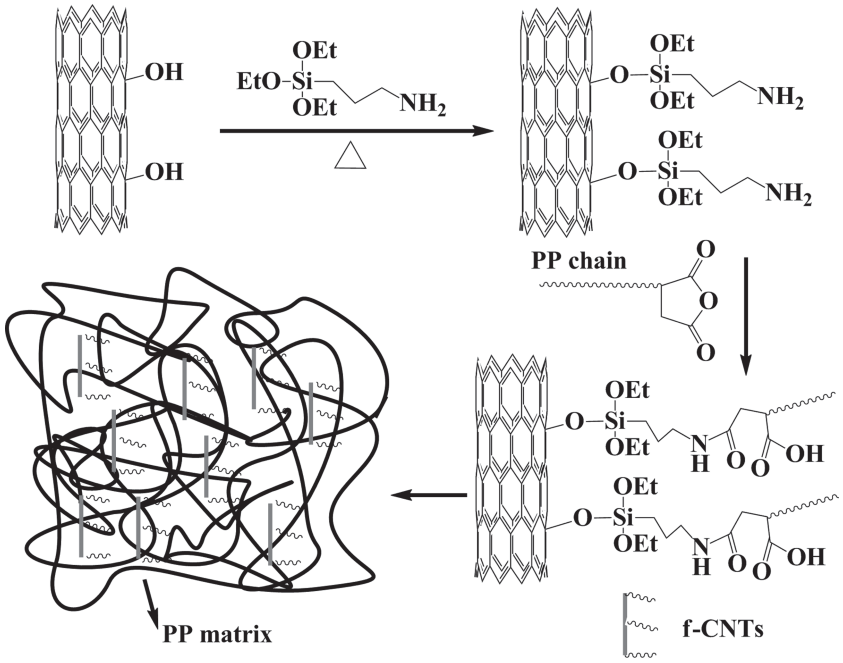

Scheme 2. Reaction route for the CNTs functionalization and the fabrication of PP PNCs.

3.2. SEM Images

The dispersion quality of the CNTs/f-CNTs in the hosting PP matrix is evaluated by SEM and the cross-sectional surface morphology of these PP PNCs (prepared from fracturing the bar shape samples after immersing in liquid nitrogen). Figure 6a,b shows that 1.0 wt% CNTs were randomly distributed in the PP matrix and an interconnected structure was formed with some aggregates. Long tubes being pulled out from the PP matrix can be clearly seen (Figure 6b), indicating a poor interfacial adhesion between the PP matrix and the untreated CNTs.[28] Figure 6c shows a smoother fracture surface when adding 1 wt% MAPP-1 into PP/1 wt% CNTs system. Magnified image (Figure 6d)

© 2014 WILEY-VCH Verlag GmbH & Co. KGaA, Weinheim

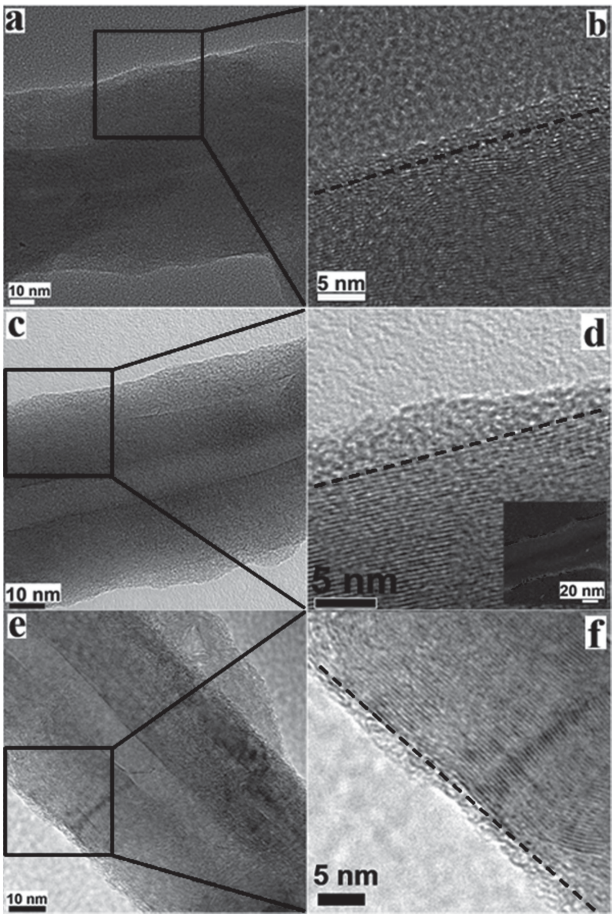

Figure 4. TEM images of: a,b) treated CNTs in the PP matrix. c,d) treated CNTs in PP matrix with MAPP-1, and insert of d) is the elemental mapping (carbon: tube structure, silicon: light grey, and oxygen: black), and e,f) treated CNTs in PP matrix with MAPP-2.

shows only the ends of untreated CNTs on the cross-sectional PP surface, indicating an enhanced interfacial interaction between CNTs and PP matrix due to the bridging

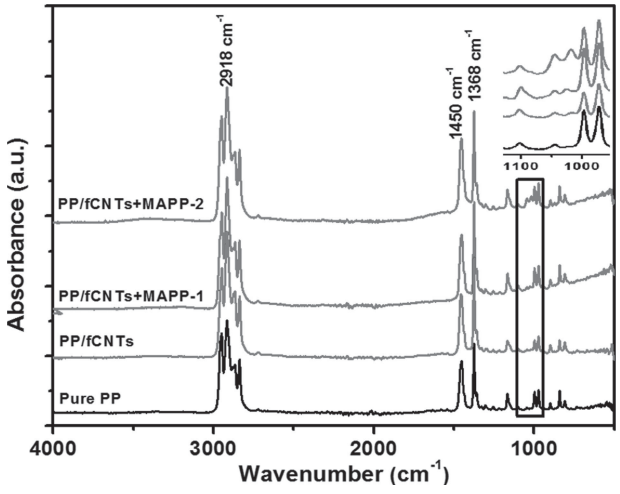

Figure 5. FTIR spectra of pure PP and its PNCs reinforced with f-CNTs with/without MAPP.

effect of MAPP-1. Shown in the SEM images (Figure 6e,f), when combining 1 wt% CNTs with 1 wt% MAPP-2, CNTs were less detached compared with pure PP, indicating a better adhesion. However, compared with MAPP-1, MAPP-2 showed a decreased adhesion to CNTs, which is probably due to less MA density caused from the higher molecular weight.

When adding 1.0 wt% f-CNTs into PP matrix, more severe agglomeration of the f-CNTs was observed in the PP matrix (Figure 7a,b), indicating worse dispersion quality in the PP matrix compared with PP/1.0 wt% CNTs. This might be caused from higher affinity among the f-CNTs than that of CNTs. However, a much smoother surface was noticed when adding MAPP (Type 1 or 2) and f-CNTs in the PP matrix. The SEM images of the fracture surface (Figure 7c,d), show that the f-CNTs were fixed by PP at two ends, indicating a much stronger interfacial interaction between the PP matrix and the f-CNTs through the coupling effect of MAPP-1. When adding 1.0 wt% MAPP-2 and 1.0 wt% f-CNTs in the PP matrix, much fewer tube ends being pulled out from the fractural surface of PP matrix were observed, which evidenced that the interfacial adhesion between the f-CNTs and the PP matrix is significantly enhanced due to the strong chemical bonding through MAPP-2, however, less intensive than the effects of MAPP-1. The difference in the MA percentage between MAPP-1 and -2 was believed to be responsible for the observed SEM morphology difference (Figure 7). Since the $\bar{M}_w$ of MAPP-2 is 10 times higher than that of MAPP-1, the higher MA group density leads to a stronger interfacial adhesion effect between PP and f-CNTs.[49]

3.3. Thermogravimetric Analysis (TGA)

Figure 8a,b shows the TGA curves of pure PP, and its nanocomposites with 1.0 wt% CNTs (or 1.0 wt% f-CNTs) loading in the presence/absence of MAPP tested under the nitrogen (Figure 8a) and air (Figure 8b) atmosphere, respectively. The initial thermal decomposition temperature (T_{ini}) is defined as the temperature at 5.0% weight loss of the tested specimen; T_{max} is defined as the temperature, at which the specimen experiences the maximum weight loss rate. These detailed thermal decomposition temperatures are shown in Table 1 and 2.

As seen in Figure 8a, all the samples investigated experience a one-step degradation from 350 to 500 °C till no residue left at around 600 °C. For pure PP, it started to decompose at 395.0 °C, and experienced a T_{max} at 450.4 °C with no residue left at 600 °C. The addition of 1.0 wt% CNTs in the hosting PP matrix significantly increased the thermal stability of PP by increasing the T_{ini} of 14.9 °C (from 395.0 to 409.9 °C) and T_{max} of 34.9 °C (from 450.4 to 485.3 °C); meanwhile, approximate 0.8 wt% char residue was observed at 600 °C. Though adding 1.0 wt% MAPP

© 2014 WILEY-VCH Verlag GmbH & Co. KGaA, Weinheim

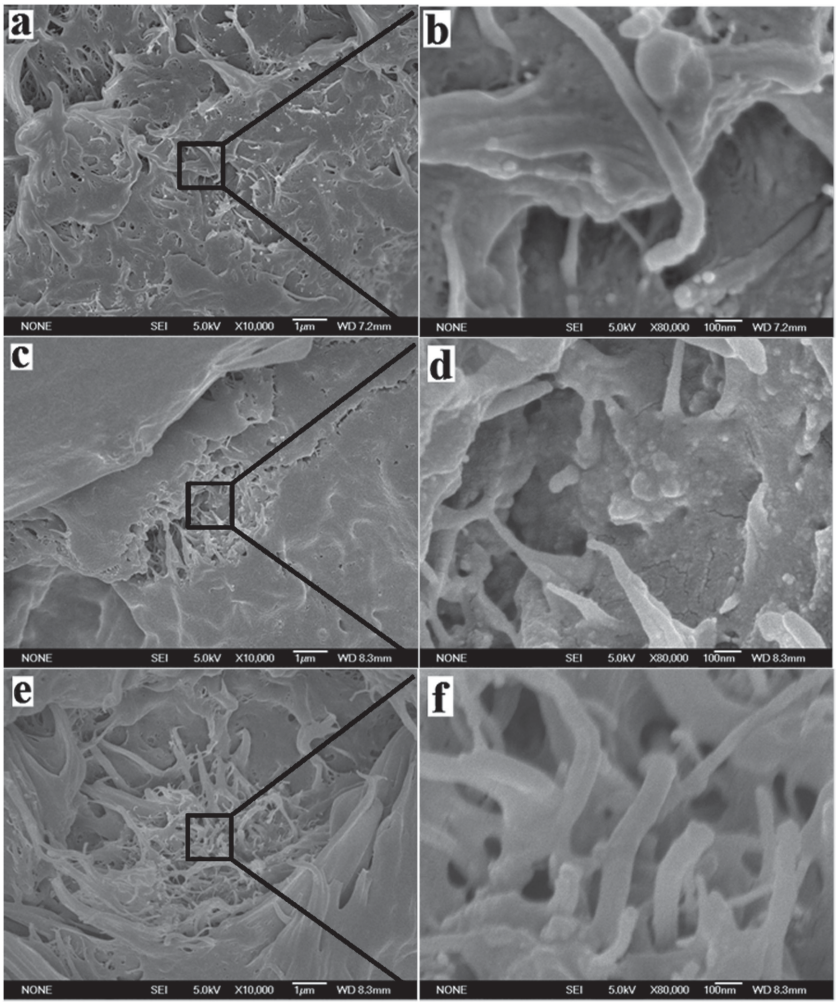

Figure 6. SEM images of polymer nanocomposites: a,b) PP/1% CNTs. c,d) PP/1.0% CNTs/1.0% MAPP-1, and e,f) PP/1.0% CNTs/1.0% MAPP-2.

(Type 1 or 2) in the PP/1.0 wt% CNTs system did not change the T_{max}, the T_{ini} was further increased noticeably (for example, the T_{ini} was increased by 19.7 °C from 409.9 to 429.6 °C when adding 1.0 wt% MAPP-1 in the PP/1% CNTs system, Table 1 and insert of Figure 8a); indicating that a more stable composite was formed in the presence of MAPP (Type 1 or 2). Compared with the PP/1.0 wt% CNTs PNCs, the increased char residue for the PP/1.0 wt% MAPP/1.0 wt% CNTs PNCs also indicated the enhanced thermal stability after adding MAPP. Usually, the introduction of small amount of MAPP in the PP matrix decreased the thermal stability of PP as reported by the lower T_{ini} arising from the relative low stability of small-molecular-weight MAPP,[59] the observed increase in T_{ini} for the PP/1% MAPP/1% CNTs PNCs confirmed that the combination of CNTs with MAPP (Type 1 or 2) increased the thermal stability of PP. The probable reason is that the increased entanglement/adhesion between CNTs and PP matrix reached by the MAPP (as evidenced by SEM images shown above) effectively offsets the lower stability of MAPP.

Compared with the T_{ini} of 409.9 °C for the PP/1% CNTs PNCs, a significant decrease (55.5 °C) in T_{ini} took place when adding 1% f-CNTs in the PP matrix (Figure 8b and Table 1, which might be caused from more free volume created by the agglomerated f-CNTs, since it is clear from SEM image (Figure 7a,b) that self-interaction among CNTs took place. Therefore, the dispersion of f-CNTs in the PP matrix became more difficult compared with CNTs. Another probable reason is that the APTES on the f-CNTs may also lead to a lower T_{ini} by causing earlier degradation compared with as-received CNTs. Previously, Luo et al. reported that the thermal stability of CNTs can be reduced upon the functionalization of CNTs.[60] Similarly, the APTES on the functionalized CNTs (f-CNTs) may also cause earlier degradation because the relative low thermal stability. The high char residue for PP/1% f-CNTs is probably caused by the agglomeration of f-CNTs, which led to more difficulty in decomposing them at high temperatures, and worse efficiency in protecting the PP matrix from earlier degradation. After adding MAPP (Type 1 or 2) in the PP/1% f-CNTs system, the T_{ini} increased sharply, for example, from 354.4 to 438.8 °C (increase of 84.4 °C) when adding 1.0 wt% MAPP-1 in the PP/1% f-CNTs PNCs. The T_{ini} is 9.2 °C higher than that of PP/1% MAPP-1/1% CNTs. In addition, the char residues of PP/1% MAPP/1% f-CNTs were higher than the counterparts of these PP/1% MAPP/1% CNTs systems, which clearly demonstrated that the f-CNTs increased the thermal stability of PP in the presence of MAPP.

The thermal oxidative degradation curves of both PP and its nanocomposites in air were shown in Figure 9a,b. In air condition, the thermal oxidative degradation of one polymeric material was dominated by oxidative dehydrogenation in association with hydrogen abstraction.[12] It is obvious that the thermal oxidative decomposition in air took place much earlier than that under an inert atmosphere due to the earlier formation of unstable radicals from the oxygen-induced decomposition.[12] T_{ini} and T_{max} were significantly decreased, for example, for pure PP, T_{ini} (266.5 °C) and T_{max} (327.2 °C) were 128.5 and 123.2 °C lower than those decomposition temperatures under an inert decomposition condition. Moreover, the residues left

© 2014 WILEY-VCH Verlag GmbH & Co. KGaA, Weinheim

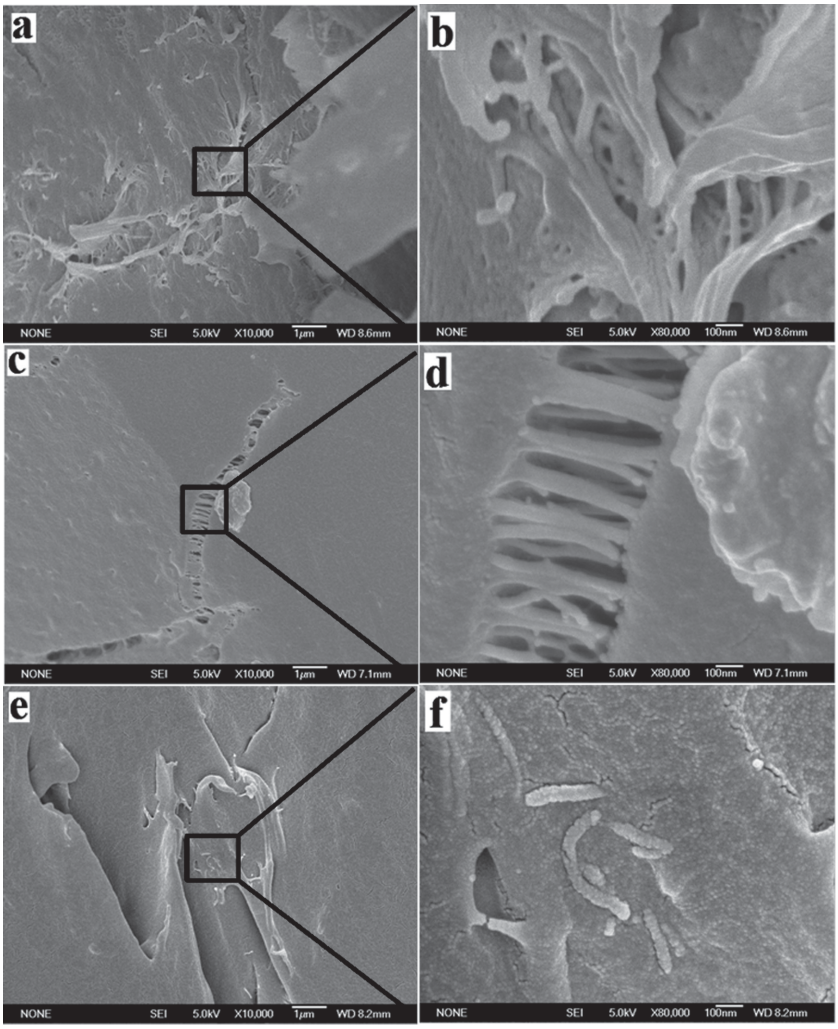

Figure 7. SEM images of polymer nanocomposites: a,b) PP/1.0% f-CNTs. c,d) PP/1.0% f-CNTs/1.0% MAPP-1, and e,f) PP/1.0% f-CNTs/1.0% MAPP-2.

from the oxidative degradation of all the specimens were less than those degraded in nitrogen at 600 °C under air. The PP/1% CNTs started to decompose at 278.4 °C, which was 11.9 °C higher than that of pure PP; meanwhile, T_{max} was significantly increased from 327.2 to 409.0 °C (increase of 81.8 °C). With further addition of 1.0 wt% MAPP (Type 1 or 2) in the PP/1% CNTs PNCs, T_{ini} further increased; i.e., from 278.4 to 306.1 °C (increase 27.7 °C) in the presence of 1.0 wt% MAPP-1. However, the T_{max} increased with adding 1.0 wt% MAPP-1 while decreased with adding 1.0 wt% MAPP-2 in the PP/1.0 wt% CNTs system (Table 2).

Compare with the PP PNCs with 1.0 wt% CNTs, T_{ini} of PP/1.0 wt% f-CNTs decreased from 278.4 to 257.8 °C (20.6 °C reduction), which was also 8.7 °C lower than that of pure PP. This observation is similar to the thermal decomposition of PP/1.0 wt% f-CNTs under nitrogen. The probable reason is also the increased the free volumes of PP arising from the agglomerated f-CNTs since the f-CNTs is hydrophilic and PP is hydrophobic;[61] which acted as defects in the PP matrix and deteriorated the thermal oxidative stability. Meanwhile, T_{max} was significantly decreased from 409.0 to 373.7 °C (35.3 °C reduction). With further addition of 1.0 wt% MAPP (Type 1 or 2) in the PP/1% CNTs, T_{ini} reversely increased; i.e., from 278.4 to 305.2 °C (increase 26.8 °C) in the presence of 1.0 wt% MAPP-1. More importantly, the T_{max} and char residues were found to be further increased with adding 1.0 wt% MAPP (Type 1 or 2) in the PP/1% f-CNTs (Table 2).

Those significant enhancements in decomposition temperatures are attributed to the improved interfacial interactions between f-CNTs and PP matrix by the coupling effects of MAPP-1. However, the less intensive improvement, when MAPP-2 was combined with CNTs, is due to the maleic anhydride grafting density difference between MAPP-1 and MAPP-2. As seen in the SEM morphology (Figure 7), stronger interfacial adhesion between f-CNTs and PP matrix through MAPP-1 leads to the requirement of more energy to decompose the PNCs in air. On the other hand, the $\bar{M}_w$ of MAPP-2 is ten times of MAPP-1, indicating longer PP chains with less dense MA grafting on the PP chain, which leads to fewer interfacial interaction spots between f-CNTs and hosting PP.

3.4. MCC Heat Release Parameters

MCC was further utilized to characterize the combustion behaviors of PP and its PNCs with CNTs/f-CNTs in the presence/absence of MAPP. Figure 10 depicted the HRR versus temperature curves and the corresponding heat release parameters are summarized in Table 3. The HRR is the single most important parameter to assess the fire hazard of one flammable material.[62] PHRR is the peak (maximum) HRR, one material can generate the highest rate of heat release under explosion to certain fire scenario (which is related to specific temperature here). In other words, the higher the PHRR is, the more dangerous one material will act under fire accident. T_{PHRR} refers to the temperature, at which the peak heat release rate occurs.

© 2014 WILEY-VCH Verlag GmbH & Co. KGaA, Weinheim

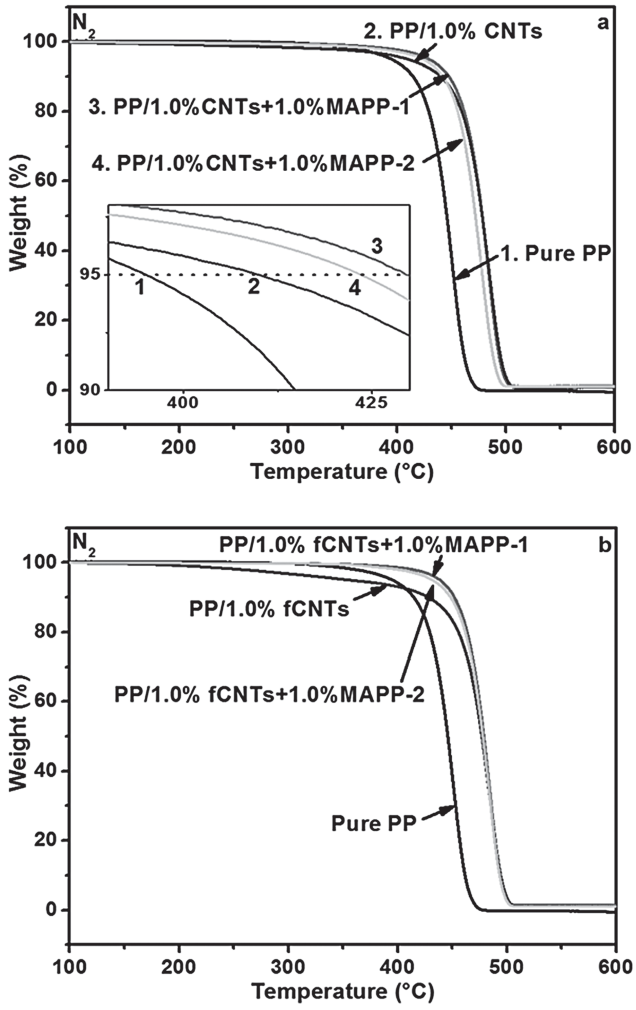

Figure 8. TGA curves of: a) pure PP, nanocomposites of PP/1.0% CNTs, nanocomposites of PP/1.0% CNTs/1.0% MAPP (1 or 2), and b) PP, nanocomposites of PP/1.0% f-CNTs, nanocomposites of PP/1.0% f-CNTs/1.0% MAPP (1 or 2) PNCs in N_2. Insert is the enlarged area at the temperatures ranged from 380–430 °C.

Pure PP is highly flammable as indicated by a PHRR of 1513.0 W g^{-1}, HRC of 1187.0 J g^{-1} K^{-1}, and T_{PHRR} of 490.4 °C. When introducing small amount of CNTs such as 1.0 wt%

Table 1. TGA data of PP and its PNCs in N_2.

Composition	T_{ini} (N_2) [°C]	T_{max} [°C]	Residue at 600 °C [%]
PP	395.0	450.4	0.0
PP/1% CNTs	409.9	485.3	0.8
PP/1% CNTs+1% MAPP-1	429.6	484.5	1.2
PP/1% CNTs+1% MAPP-2	423.5	478.2	1.0
PP/1% f-CNTs	354.4	482.4	1.5
PP/1% f-CNTs+1% MAPP-1	438.8	484.5	1.5
PP/1% f-CNTs+1% MAPP-2	431.9	484.5	1.1

Table 2. TGA data of PP and its PNCs in air.

Composition	T_{ini} (air) [°C]	T_{max} [°C]	Residue at 500 °C [%]
PP	266.5	327.2	0.0
PP/1% CNTs	278.4	409.0	0.7
PP/1% CNTs+1% MAPP-1	306.1	411.1	0.9
PP/1% CNTs+1% MAPP-2	295.4	400.5	0.6
PP/1% f-CNTs	257.8	373.7	0.3
PP/1% f-CNTs+1% MAPP-1	305.2	417.4	1.2
PP/1% f-CNTs+1% MAPP-2	300.8	410.4	0.7

in the PP matrix, the PHRR decreased sharply from 1513.0 to 1136.0 W g^{-1} (24.9% reduction); and HRC decreased from 1187.0 to 1058.0 J g^{-1} K^{-1}.

Meanwhile, the T_{PHRR} was decreased from 490.4 to 482.1 °C. Further addition of 1.0 wt% MAPP-1 was observed

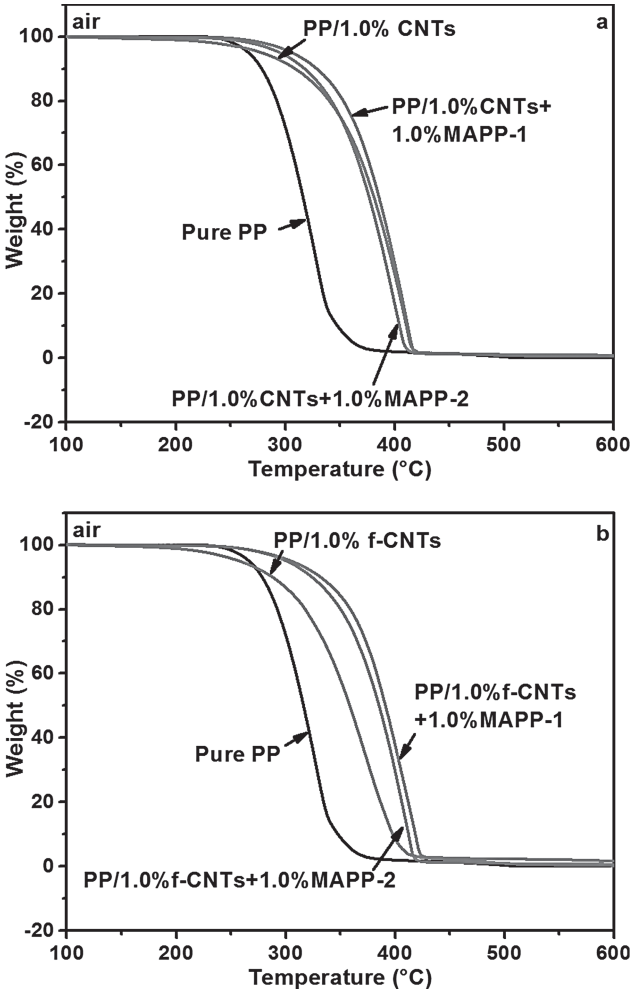

Figure 9. TGA curves of (a) PP, nanocomposites of PP/1.0% CNTs, nanocomposites of PP/1.0% CNTs/1.0% MAPP (1 or 2), and (b) PP, nanocomposites of PP/1.0% f-CNTs, nanocomposites of PP/1.0% f-CNTs/1.0% MAPP (1 or 2) PNCs in air.

© 2014 WILEY-VCH Verlag GmbH & Co. KGaA, Weinheim

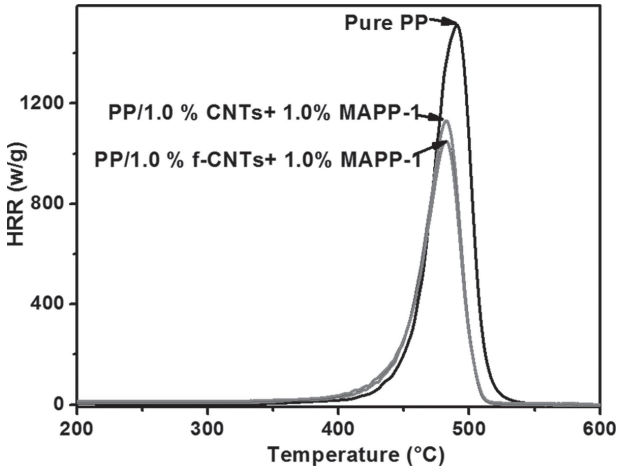

Figure 10. HRR curves as a function of temperature for PP, nanocomposites of PP/1% MAPP-1/CNTs, and nanocomposites of PP/1% MAPP-1/f-CNTs.

to have limited effect on further decrease the combustion rate of PP as indicated by a PHRR of 1130.0 W g^{-1} and a HRC of 1053.0 J g^{-1} K^{-1}. However, adding 1.0 wt% MAPP-2 into PP/1.0 wt% CNTs system increased the combustion rate of PP: PHRR increased from 1136.0 to 1200.0 W g^{-1}; and HRC increased from 1058.0 to 1119.0 J g^{-1} K^{-1}.

In the case of the PP/1.0 wt% f-CNTs PNCs, PHRR was decreased to1089.0 W g^{-1} (28.0% reduction), and HRC was decreased to 1014.0 J g^{-1} K^{-1}. The decrease in combustion rate is apparently attributed to the flame-retardant effect of silicon-containing compounds on the surface of CNTs. A barrier effect from these silicon compounds was believed to be responsible for the decreased HRR. During the decomposition, heat and mass transfers between gas- and condensed-phases were slowed down by forming an insulating layer on the outer surface of PP during the burning process.[13,37]

In the case of the PP/1.0 wt% f-CNTs PNCs in the presence of 1.0 wt% MAPP-1, PHRR was further decreased to1046.0 W g^{-1} (30.9% reduction), and HRC was decreased to 975.7 J g^{-1} K^{-1}. This suggests that the dispersion quality of CNTs in the PP matrix through MAPP-1 can lead to a better flammability reduction ability since the interfacial adhesion shows limited effect on reducing the flammability here (Table 3). However, when MAPP-1 was replaced by MAPP-2 in the PP/1.0% f-CNTs system, the increased PHRR and HRC (Table 3) were probably due to the induced more free volume by the higher-molecular-weight MAPP-2[46] rather than the decreased interfacial interactions. One can be also observed that FWHH of the PP/1.0% f-CNTs+1.0% MAPP-1(33.2 s) was much wider than that of pure PP (24.2 s, Table 4), further indicating a longer combustion period upon introducing the MAPP-1 and f-CNTs in the PP matrix. This is another sign of lower fire hazard of the PP/1.0% f-CNTs+1.0% MAPP-1 PNCs.

Table 3. MCC data of the measured samples.

Composition	HRC [J g^{-1} K^{-1}]	PHRR [W g^{-1}]	PHRR reduction [%]	T_{PHRR} [°C]	FWHH [s]
PP	1187.0	1513.0	–	490.4	24.2
PP/1% CNTs	1058.0	1136.0	24.9	482.1	31.6
PP/1% CNTs+1% MAPP-1	1053.0	1130.0	25.3	482.0	32.2
PP/1% CNTs+1% MAPP-2	1119.0	1200.0	20.7	480.7	30.6
PP/1% f-CNTs	1014.0	1089.0	28.0	481.2	32.1
PP/1% f-CNTs+1% MAPP-1	975.7	1046.0	30.9	482.2	33.2
PP/1% f-CNTs+1% MAPP-2	1136.0	1220.0	19.4	481.1	30.6

Table 4. DSC data of pure PP, PP/CNTs, and PP/CNTs/MAPP PNCs.

Composition	T_m [°C]	ΔH_m [J g^{-1}]	T_c [°C]	ΔH_c [J g^{-1}]	F_c [%]
PP	150.7	101.8	121.3	104.7	48.7
PP/1% CNTs	149.1	83.3	119.2	88.8	40.3
PP/1% CNTs+1% MAPP-1	150.3	74.4	119.2	80.6	36.3
PP/1% CNTs+1% MAPP-2	150.6	88.2	120.1	89.7	42.6
PP/1% f-CNTs	146.1	77.2	112.5	83.4	37.3
PP/1% f-CNTs+1% MAPP-1	148.5	77.7	112.5	85.4	38.0
PP/1% f-CNTs+1% MAPP-2	150.7	92.1	120.5	98.1	44.5

© 2014 WILEY-VCH Verlag GmbH & Co. KGaA, Weinheim

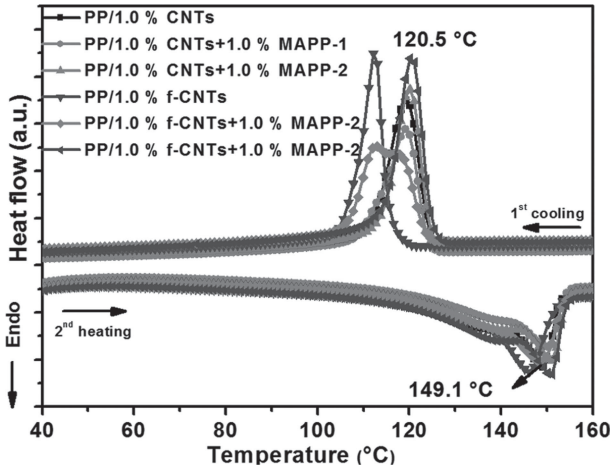

Figure 11. DSC curves of PP/1% CNTs, nanocomposites of PP/1% f-CNTs, nanocomposites of PP/1.0% CNTs/1% MAPP (1 or 2), and PP/1.0% f-CNTs/1% MAPP (1 or 2).

3.5. Differential Scanning Calorimetry (DSC)

DSC endothermic and exothermic curves (Figure 11) depict the melting/crystallization behaviors of pure PP and PP/CNTs nanocomposites. Detailed data including melting peak temperature, T_m; crystalline peak temperature, T_c; heat of fusion, ΔH_m; and crystalline fraction, F_c; are summarized in Table 4. The F_c of the studied samples was determined according to Equation 1:

$$F_c = \Delta H_m / [\Delta H_m^{\circ}(1-x)] \quad (1)$$

where, ΔH_m is the measured heat of fusion (integration of the melting peak area under the baseline of DSC curves); ΔH_m° is the heat of fusion of 100% crystalline PP (here, the theoretical value of ΔH_m° used is 209 J g^{-1}).[63,64] Pure PP exhibits a T_m at 150.7 °C and a ΔH_m of 101.8 J g^{-1} with F_c of 48.7%. When 1.0 wt% CNTs was introduced in the PP matrix, the T_m was slightly decreased (149.1 °C); however, ΔH_m was significantly decreased from 101.8 to 83.3 J g^{-1}, corresponding to a decreased F_c of 40.3%. When the addition of 1.0 wt% MAPP (Type 1 or 2), T_m stayed unchanged compared with that of pure PP; however, ΔH_m was further decreased to 74.4 J g^{-1} for adding 1.0 wt% MAPP-1, and increased to 88.2 J g^{-1} for adding 1.0 wt% MAPP-2, respectively. The corresponding F_c is 36.3 and 42.6%. For either the PP/1% CNTs or PP/1% CNTs/1% MAPP (Type 1 or 2), there is no obvious change of T_c, indicating that no strong restriction of PP crystallization was occurred. When adding 1.0 wt% f-CNTs in the PP matrix, T_m decreased to 146.1 °C and T_c decreased to 112.5 °C, which represents 4.6 and 8.8 °C decrease, respectively. Meanwhile, the F_c is decreased to 37.3%. This is clear that the crystallization of PP was restricted by 1.0 wt% f-CNTs. In combination with 1.0 wt% f-CNTs and 1.0 wt% MAPP-1, all these parameters were slightly changed as shown in Table 4. However, when combining 1% f-CNTs and 1% MAPP-2, the ΔH_m was significantly increased 92.1 J g^{-1}, corresponding to an F_c of 44.5%. Meanwhile, T_m (146.1 °C) and T_c (120.5 °C) are similar to those of pure PP.

Usually, for semicrystalline polymers like PP, the addition of CNTs leads to an earlier crystallization (increase T_c) compared to pure polymer because the heterogeneous nucleating effect of CNTs can accelerate the crystallization when polymer is cooled upon melt.[16,65] Nonetheless, the decrease of T_c here is probably attributed to the non-crystallizable barrier effect of the agglomerated f-CNTs in the PP matrix.[65] Therefore, the fillers can act as non-crystallizable barriers to disturb the crystal growth of polymer crystallization, which inversely decelerates the crystallization. Furthermore, the fillers may also hinder the mobility of polymer chains, which in turn restricts the growth of the crystallites.[66,67] Through the SEM image in Figure 6a,b, it is clear that the f-CNTs can also form an interconnected network structure, which well explains "why the addition of 1.0% CNTs can significantly hinder the crystallization of hosting PP by lowering the T_c."[68]

In addition to the decreased T_c, the peak broadening effects in the PP/1.0% f-CNTs, and PP/1.0% f-CNTs/1.0% MAPP-1 PNCs were also observed during the exothermic crystallization cycle, indicating the formation of imperfect polymer crystallites and the size distribution broadening effect of thus formed crystallites.[69,70] The T_c (112.5 °C) of the PP/1.0 wt% f-CNTs/1.0 wt% MAPP-1 was further decreased compared with that (119.2 °C) of the PP/1.0 wt% CNTs, indicating a stronger barrier effect to the PP crystallization, while T_c was not significantly changed when MAPP-2 (120.5 °C) was introduced in the PP matrix since the larger free volume has been introduced (Figure 11).

3.6. Melt Rheological Behaviors

The melt rheological behaviors of pure PP and its PNCs at 200 °C were investigated by studying the complex viscosity (η^*), storage moduli (G'), and loss moduli (G'') as a function of oscillation frequency (Hz). Generally, different melting rheological behaviors indicate the internal structure of the polymers or their PNCs including percolated network structure, particle dispersion state, and the interfacial interaction between polymer matrix and the nanofillers.[71] Figure 12a shows the complex viscosity (η^*) of the melts of pure PP and its PNCs. Pure PP demonstrated a nearly constant η^* at low-frequency range (0.1–1.0 Hz) and decreased η^* with further increasing frequency range till 100 Hz, indicating a typical Newtonian-flow behavior at low frequencies and shear thinning behavior at high frequencies.[57] However, when 1.0 wt% CNTs were added in the PP matrix, similar trend of η^* was observed except a relatively

© 2014 WILEY-VCH Verlag GmbH & Co. KGaA, Weinheim

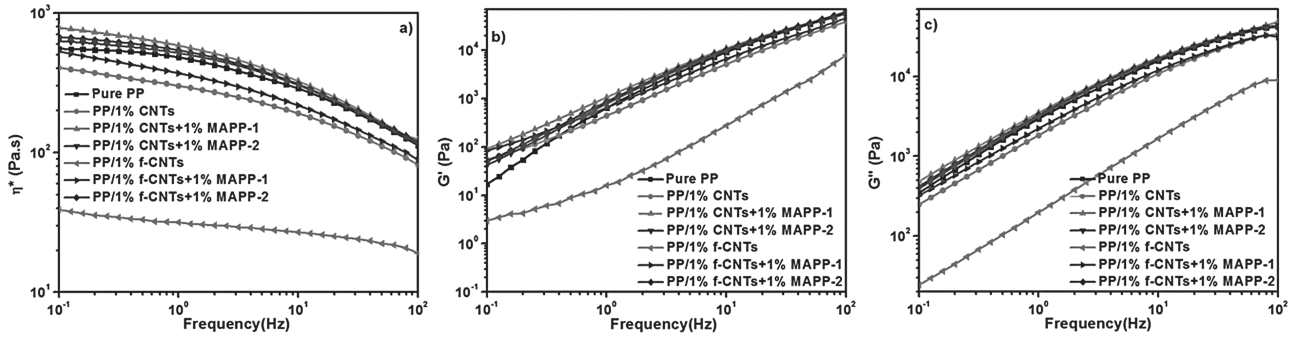

Figure 12. a) Complex viscosity. b) storage modulus, and c) loss modulus of PP, PP/1.0% CNTs/1.0% MAPP (1or2), and PP /1.0% f-CNTs/1.0% MAPP (1 or 2) PNCs melts at 200 °C.

lower η^* than that of pure PP and a monotonic decreased η^* values with increasing the oscillation frequency, indicating a typical shear thinning behavior. Usually, the addition of small amount of nanofillers in the PP matrix can increase the η^* because of the impedance of the polymer chains by the nanofillers.[57] Therefore, the decreased η^* by adding 1.0 wt% CNTs can only be explained by the existence of large free volume in the polymer matrix as evidenced by the CNTs agglomeration from the SEM image (Figure 6a,b).[61] When additional 1.0 wt% MAPP (Type 1 or 2) is introduced in the PP/1% CNTs system, the increased η^* was observed. The higher η^* with adding 1.0 wt% MAPP-1 than 1.0 wt% MAPP-2 is apparently caused by the higher grafted density of MA functional groups from the low-molecular-weight MAPP-1.[59] As the higher MA functional groups concentration can result in stronger entanglement between the CNTs and PP matrix through the coupling effect by MAPP, the η^* was increased correspondingly.

After the functionalization of CNTs, the addition of f-CNTs significantly decreased the η^* (Figure 11a), which is probably attributed to the further agglomeration of CNTs after the APTES functionalization since the CNTs (SEM images, Figure 7). As the surface of f-CNTs was "wrapped" with chemically bonded APTES (TEM images, Figure 1c,d), the enlarged polarity of f-CNTs can lead self-aggregation, which would be much more difficult to be dispersed in the inert PP matrix compared with the untreated CNTs. On the other hand, the lubricating effect imparted from the surfactant effect of APTES may also contribute to the decreased viscosity. Therefore, much higher free volume was formed in the PP matrix after the addition of 1.0 wt% f-CNTs, which resulted in the significantly decreased η^*. After the addition of MAPP (Type 1 or 2), the PP/MAPP/f-CNTs system demonstrated a similar η^* as the PP/MAPP/CNTs, indicating that the incorporation of MAPP remarkably enhanced the dispersion of f-CNTs in the PP matrix. It must be noted that the addition of MAPP-1 into PP/1% f-CNTs system led to a slightly decreased η^* than that of pure PP, which is favorable for lowing the energy consumption during the process of the PNCs.

When adding the combined 1.0 wt% f-CNTs and 1.0 wt% MAPP (Type 1 or 2) in the PP matrix, both G' and G'' are much higher than those of the PP/1.0 wt% f-CNTs PNCs, indicating a much better dispersion quality upon the introduction of 1.0 wt% MAPP (Type 1 or 2). From the SEM images (Figure 7c–f), it is clear that the f-CNTs were well dispersed in the PP matrix, and few tubes have been pulled out from the fracture surface. This suggests that a strong interaction between the f-CNTs and PP matrix through the bridging effects of MAPP (Type 1 and 2) is responsible for the enhanced G' and G''.[72]

4. Conclusion

PP nanocomposites reinforced with functionalized multiwall CNTs in the presence of coupling agent MAPP have been successfully fabricated through an ex-situ solution blending approach. Increased thermal stability of PP nanocomposites with only 1.0 wt% CNTs has been observed, and thermal stability was further increased by adding MAPP-1 (high MA density) in the PP/CNTs system. The flame retardancy of PP was improved by the combination of f-CNTs and MAPP-1, which is attributed to the better dispersion of f-CNTs and the introduced silicon-containing APTES. Meanwhile, the surfactant (MAPP) molecular-weight-dependent thermal behavior (≈44 °C increase in the initial thermal decomposition temperature compared with pure PP through combining 1.0 wt% MAPP-1 with 1.0 wt% f-CNTs), flame retardancy (more than 30% reduction in HRR through combining 1.0 wt% MAPP-1 with 1.0 wt% f-CNTs), and melting rheological behaviors have been reported to provide insight to the systems for practical applications such as flame-retardant fibers[73] for aerospace usage.[74]

Acknowledgements: This project was supported by Baker Hughes and National Science Foundation – Nanoscale Interdisciplinary Research Team and Materials Processing and Manufacturing (CMMI 10–30755) to purchase TGA and DSC. The authors are thankful to the Open Funding from State Key Laboratory of Organic-Inorganic Composites, BUCT.

© 2014 WILEY-VCH Verlag GmbH & Co. KGaA, Weinheim

Received: September 27, 2013; Revised: November 30, 2013; Published online: January 13, 2014; DOI: 10.1002/macp.201300608

Keywords: carbon nanotubes; flame-retardant materials; maleic-anhydride-grafted polypropylene; surface modification; thermal stability

[1] M. F. Yu, B. S. Files, S. Arepalli, R. S. Ruoff, *Phys. Rev. Lett.* **2000**, *84*, 5552.
[2] M. F. Yu, O. Lourie, M. J. Dyer, K. Moloni, T. F. Kelly, R. S. Ruoff, *Science* **2000**, *287*, 637.
[3] Q. Zhao, M. D. Frogley, H. D. Wagner, *Compos. Sci. Technol.* **2001**, *61*, 2139.
[4] B. Lukic, J. W. Seo, R. R. Bacsa, S. Delpeux, F. Béguin, G. Bister, A. Fonseca, J. B. Nagy, A. Kis, S. Jeney, *Nano Lett.* **2005**, *5*, 2074.
[5] W. Li, X. Wang, Z. Chen, M. Waje, Y. Yan, *Langmuir* **2005**, *21*, 9386.
[6] S. J. Yang, J. Y. Choi, H. K. Chae, J. H. Cho, K. S. Nahm, C. R. Park, *Chem. Mater.* **2009**, *21*, 1893.
[7] K. E. Tettey, M. Q. Yee, D. Lee, *ACS Appl. Mater. Interfaces* **2010**, *2*, 2646.
[8] H. Wei, H. Gu, J. Guo, S. Wei, Z. Guo, *J. Electrochem. Soc.* **2013**, *160*, G3038.
[9] H. Wei, H. Gu, J. Guo, S. Wei, Z. Guo, *ECS J. Solid State Sci. Technol.* **2013**, *2*, M3008.
[10] L. F. Cui, L. Hu, J. W. Choi, Y. Cui, *ACS Nano* **2010**, *4*, 3671.
[11] G. Beyer, *Fire Mater.* **2002**, *26*, 291.
[12] T. Kashiwagi, E. Grulke, J. Hilding, R. Harris, W. Awad, J. Douglas, *Macromol. Rapid Commun.* **2002**, *23*, 761.
[13] T. Kashiwagi, E. Grulke, J. Hilding, K. Groth, R. Harris, K. Butler, J. Shields, S. Kharchenko, J. Douglas, *Polymer* **2004**, *45*, 4227.
[14] T. Kashiwagi, F. Du, J. F. Douglas, K. I. Winey, R. H. Harris, J. R. Shields, *Nat. Mater.* **2005**, *4*, 928.
[15] T. Kashiwagi, M. Mu, K. Winey, B. Cipriano, S. Raghavan, S. Pack, M. Rafailovich, Y. Yang, E. Grulke, J. Shields, *Polymer* **2008**, *49*, 4358.
[16] B. X. Yang, K. P. Pramoda, G. Q. Xu, S. H. Goh, *Adv. Funct. Mater.* **2007**, *17*, 2062.
[17] A. A. Koval'chuk, V. G. Shevchenko, A. N. Shchegolikhin, P. M. Nedorezova, A. N. Klyamkina, A. M. Aladyshev, *Macromolecules* **2008**, *41*, 7536.
[18] Y. Li, H. Shimizu, *Macromolecules* **2009**, *42*, 2587.
[19] P. Liu, K. L. White, H. Sugiyama, J. Xi, T. Higuchi, T. Hoshino, R. Ishige, H. Jinnai, A. Takahara, H.-J. Sue, *Macromolecules* **2013**, *46*, 463.
[20] H. Gu, S. Tadakamalla, X. Zhang, Y. Huang, Y. Jiang, H. A. Colorado, Z. Luo, S. Wei, Z. Guo, *J. Mater. Chem. C* **2013**, *1*, 729.
[21] P. Song, L. Xu, Z. Guo, Y. Zhang, Z. Fang, *J. Mater. Chem.* **2008**, *18*, 5083.
[22] Y. Li, J. Zhu, S. Wei, J. Ryu, Q. Wang, L. Sun, Z. Guo, *Macromol. Chem. Phys.* **2011**, *212*, 2429.
[23] J. Zhu, X. Zhang, N. Haldolaarachchige, Q. Wang, Z. Luo, J. Ryu, D. P. Young, S. Wei, Z. Guo, *J. Mater. Chem.* **2012**, *22*, 4996.
[24] H. Geng, R. Rosen, B. Zheng, H. Shimoda, L. Fleming, J. Liu, O. Zhou, *Adv. Mater.* **2002**, *14*, 1387.
[25] Z. Zhou, S. Wang, L. Lu, Y. Zhang, *Compos. Sci. Technol.* **2008**, *68*, 1727.
[26] W. S. Tseng, C. Y. Tseng, P. K. Chuang, A. Y. Lo, C. T. Kuo, *J. Phys. Chem. C* **2008**, *112*, 18431.
[27] B. X. Yang, J. H. Shi, K. Pramoda, S. H. Goh, *Compos. Sci. Technol.* **2008**, *68*, 2490.
[28] G. Farzi, S. Akbar, E. Beyou, P. Cassagnau, F. Melis, *Polymer* **2009**, *50*, 5901.
[29] J. H. Lee, J. Kathi, K. Y. Rhee, J. H. Lee, *Polym. Eng. Sci.* **2010**, *50*, 1433.
[30] S. Barrau, P. Demont, E. Perez, A. Peigney, C. Laurent, C. Lacabanne, *Macromolecules* **2003**, *36*, 9678.
[31] R. Ramasubramaniam, J. Chen, H. Liu, *Appl. Phys. Lett.* **2003**, *83*, 2928.
[32] R. Haggenmueller, W. Zhou, J. Fischer, K. Winey, *J. Nanosci. Nanotechnol.* **2003**, *3*, 105.
[33] F. Du, R. C. Scogna, W. Zhou, S. Brand, J. E. Fischer, K. I. Winey, *Macromolecules* **2004**, *37*, 9048.
[34] M. Biercuk, M. C. Llaguno, M. Radosavljevic, J. Hyun, A. T. Johnson, J. E. Fischer, *Appl. Phys. Lett.* **2002**, *80*, 2767.
[35] Y. Tang, J. Zhuge, J. Lawrence, J. Mckee, J. Gou, C. Ibeh, Y. Hu, *Polym. Degrad. Stab.* **2011**, *96*, 760.
[36] E. Choi, J. Brooks, D. Eaton, M. Al-Haik, M. Hussaini, H. Garmestani, D. Li, K. Dahmen, *J. Appl. Phys.* **2003**, *94*, 6034.
[37] T. Kashiwagi, F. Du, K. I. Winey, K. M. Groth, J. R. Shields, S. P. Bellayer, H. Kim, J. F. Douglas, *Polymer* **2005**, *46*, 471.
[38] D. McIntosh, V. N. Khabashesku, E. V. Barrera, *Chem. Mater.* **2006**, *18*, 4561.
[39] D. McIntosh, V. N. Khabashesku, E. V. Barrera, *J. Phys. Chem. C* **2007**, *111*, 1592.
[40] J. Zhu, S. Wei, J. Ryu, M. Budhathoki, G. Liang, Z. Guo, *J. Mater. Chem.* **2010**, *20*, 4937.
[41] L. Vaisman, G. Marom, H. D. Wagner, *Adv. Funct. Mater.* **2006**, *16*, 357.
[42] S. S. Kim, P. B. Amama, T. S. Fisher, *J. Phys. Chem. C* **2010**, *114*, 9596.
[43] P.-C. Ma, N. A. Siddiqui, G. Marom, J.-K. Kim, *Compos. Part A* **2010**, *41*, 1345.
[44] C. Lei, D. Chen, B. Wu, Y. Xu, S. Li, W. Huang, *J. Appl. Polym. Sci.* **2011**, *121*, 3724.
[45] J.-M. Thomassin, I. Huynen, R. Jerome, C. Detrembleur, *Polymer* **2010**, *51*, 115.
[46] J. Zhu, Q. He, Z. Luo, A. Khasanov, Y. Li, L. Sun, Q. Wang, S. Wei, Z. Guo, *J. Mater. Chem.* **2012**, *22*, 15928.
[47] Q. He, T. Yuan, S. Wei, N. Haldolaarachchige, Z. Luo, D. P. Young, A. Khasanov, Z. Guo, *Angew. Chem. Int. Ed.* **2012**, *51*, 8842.
[48] Q. He, T. Yuan, Z. Luo, N. Haldolaarachchige, D. P. Young, S. Wei, Z. Guo, *Chem. Commun.* **2013**, *49*, 2679.
[49] Q. He, T. Yuan, X. Zhang, Z. Luo, N. Haldolaarachchige, L. Sun, D. P. Young, S. Wei, Z. Guo, *Macromolecules* **2013**, *46*, 2357.
[50] S. Morlat, B. Mailhot, D. Gonzalez, J. L. Gardette, *Chem. Mater.* **2004**, *16*, 377.
[51] P. J. Purohit, J. E. Huacuja-Sánchez, D. Y. Wang, F. Emmerling, A. Thünemann, G. Heinrich, A. Schönhals, *Macromolecules* **2011**, *44*, 4342.
[52] M. C. Hsiao, S. H. Liao, Y. F. Lin, C. C. Weng, H. M. Tsai, C. C. M. Ma, S. H. Lee, M. Y. Yen, P. I. Liu, *Energy Environ. Sci.* **2011**, *4*, 543.
[53] K. Prashantha, J. Soulestin, M. Lacrampe, M. Claes, G. Dupin, P. Krawczak, *Express Polym. Lett.* **2008**, *2*, 735.
[54] V. Datsyuk, M. Kalyva, K. Papagelis, J. Parthenios, D. Tasis, A. Siokou, I. Kallitsis, C. Galiotis, *Carbon* **2008**, *46*, 833.
[55] A. Simon, T. Cohen-Bouhacina, M. Porte, J. Aime, C. Baquey, *J. Colloid Interface Sci.* **2002**, *251*, 278.

© 2014 WILEY-VCH Verlag GmbH & Co. KGaA, Weinheim

[56] C. Orr, J. Cernohous, P. Guegan, A. Hirao, H. Jeon, C. Macosko, *Polymer* **2001**, *42*, 8171.
[57] J. Zhu, S. Wei, Y. Li, L. Sun, N. Haldolaarachchige, D. P. Young, C. Southworth, A. Khasanov, Z. Luo, Z. Guo, *Macromolecules* **2011**, *44*, 4382.
[58] R. Tian, O. Seitz, M. Li, W. Hu, Y. J. Chabal, J. Gao, *Langmuir* **2010**, *26*, 4563.
[59] Q. He, T. Yuan, S. Wei, Z. Guo, *J. Mater. Chem. A* **2013**, *1*, 13064.
[60] Z. Luo, A. Oki, L. Carson, L. Adams, G. Neelgund, N. Soboyejo, G. Regisford, M. Stewart, K. Hibbert, G. Beharie, C. Kelly-Brown, P. Traisawatwong, *Chem. Phys. Lett.* **2011**, *513*, 88.
[61] H. Cong, M. Radosz, B. F. Towler, Y. Shen, *Sep. Purif. Technol.* **2007**, *55*, 281.
[62] V. Babrauskas, R. D. Peacock, *Fire Safety J.* **1992**, *18*, 255.
[63] E. D. Carlson, M. T. Krejchi, C. D. Shah, T. Terakawa, R. M. Waymouth, G. G. Fuller, *Macromolecules* **1998**, *31*, 5343.
[64] A. Rozanski, A. Galeski, M. Debowska, *Macromolecules* **2011**, *44*, 20.
[65] D. Xu, Z. Wang, *Polymer* **2008**, *49*, 330.
[66] T. Fornes, D. Paul, *Polymer* **2003**, *44*, 3945.
[67] D. Homminga, B. Goderis, I. Dolbnya, H. Reynaers, G. Groeninckx, *Polymer* **2005**, *46*, 11359.
[68] J. Sandler, J. Kirk, I. Kinloch, M. Shaffer, A. Windle, *Polymer* **2003**, *44*, 5893.
[69] M. Trujillo, M. Arnal, A. Müller, E. Laredo, St. Bredeau, D. Bonduel, P. Dubois, *Macromolecules* **2007**, *40*, 6268.
[70] A. A. Koval'chuk, A. N. Shchegolikhin, V. G. Shevchenko, P. M. Nedorezova, A. N. Klyamkina, A. M. Aladyshev, *Macromolecules* **2008**, *41*, 3149.
[71] S. H. Lee, E. N. R. Cho, S. H. Jeon, J. R. Youn, *Carbon* **2007**, *45*, 2810.
[72] P. Pötschke, M. Abdel-Goad, I. Alig, S. Dudkin, D. Lellinger, *Polymer* **2004**, *45*, 8863.
[73] A. R. Horrocks, *Polym. Degrad. Stab.* **2011**, *96*, 377.
[74] J. Njuguna, K. Pielichowski, *Adv. Eng. Mater.* **2003**, *5*, 769.

© 2014 WILEY-VCH Verlag GmbH & Co. KGaA, Weinheim